

Anomalous large negative magnetoresistance in transition-metal decorated graphene: Evidence for electron-hole puddles

Chinmoy Majumder, Shatabda Bhattacharya, and Shyamal K. Saha*

School of Materials Sciences, Indian Association for the Cultivation of Science, Jadavpur, Kolkata 700032, India

 (Received 8 August 2018; revised manuscript received 27 September 2018; published 8 January 2019)

Study of electron transport in chemically synthesized graphene (CSG) under magnetic field and its magnetization due to the presence of a transition-metal (TM) atom on its surface is indeed an interesting area of research in condensed-matter physics. In the last few years, several theoretical along with a few experimental results have been reported on magnetotransport in CSG, however the interaction of conduction electrons with the induced magnetic moments arising due to charge-transfer effect when a TM atom is placed on the CSG surface is poorly understood. In the present paper, CSG has been decorated by dilute concentration of the TM (Ni, Co) atom to investigate the interaction of the conduction electron and induced magnetic moment in CSG due to the presence of the TM atom and their effect on overall magnetotransport behavior. Large positive magnetoresistance (MR) is obtained in CSG over the entire temperature and field range, however in the case of TM decorated CSG (TM-CSG) a dramatic change in MR (from positive to negative) is observed in the high-field region after 30 K. The positive MR in CSG arises due to wave-function shrinkage and the large negative MR is explained in TM-CSG by the electron-hole ($e-h$) puddle generated in CSG due to charge impurity and disorder created due to the presence of the TM atom on the CSG surface. A magnetic hysteresis loop up to 5 K also confirms the magnetic moment generated in CSG as a result of charge transfer from the TM atom to CSG.

DOI: [10.1103/PhysRevB.99.045408](https://doi.org/10.1103/PhysRevB.99.045408)

I. INTRODUCTION

Since its discovery, intensive research has been carried out to investigate the charge transport through chemically synthesized graphene (CSG), a gapless semiconductor considering an electron as a relativistic particle [1–4]. During the last few years, several theorists have reported that a charge cloud from the s orbital of a transition metal (TM) is partially transferred to its d orbital and the rest is transferred to the CSG p orbital when a TM atom is placed on the CSG surface [5–7]. Because of this charge-transfer effect, a potential barrier and an antiferromagnetic interaction are created at the TM-CSG interface [5,8,9]. Some experimental results are already available in the literature to support these theoretical predictions [10–12]. TMs containing magnetic nanostructures are also grown on the CSG surface to investigate very interesting magnetic properties invoked in CSG due to this charge-transfer effect [4,13–18]. The unique feature of this charge-transfer effect is that a ferrimagnetic transition is observed when an ultrathin layer of antiferromagnetic material is grown on the CSG surface, however a perfect ferromagnetic material shows antiferromagnetic behavior [11,19]. For example, an ultrathin layer of Co grown on CSG shows antiferromagnetic behavior whereas antiferromagnetic Ni(OH)₂ grown on CSG shows ferrimagnetic behavior [10–12,19]. Subsequently, a few more studies have been carried out to investigate magnetic properties in CSG due to this charge-transfer effect [20,21].

Although intensive studies on magnetic properties in CSG due to charge-transfer or proximity effect due to the presence of TM have already been carried out, the field remains unexplored, particularly the charge transport in CSG due to interaction of conduction electrons with the induced magnetic moment in CSG generated as a result of charge-transfer or proximity effect when CSG is decorated with TM. One of the main reasons is perhaps the limitation in fabrication of TM decorated CSG by physical technique. On the other hand, CSG is very promising to investigate these interesting effects of interaction of this induced magnetic moment with conduction electrons on charge transport in spite of some difficulties arising due to some defect states generated in CSG. To investigate the detailed charge transport under magnetic field as a result of interaction of conduction electrons with the induced magnetic moment in the present paper, chemically synthesized CSG has been decorated with TM (Co, Ni) at very dilute concentration. The results are also compared with pristine CSG to understand the role of induced magnetic moment on charge transport in CSG. It is seen that a giant positive magnetoresistance (MR) which decreases with increasing temperature is observed in pristine CSG whereas a transition from positive to large negative MR occurs in the case of TM decorated CSG. The MR behavior in pristine CSG is explained by the wave-function shrinkage model, however the origin of large negative MR and the transition from positive to negative MR in the case of TM decorated CSG has been analyzed by the electron-hole ($e-h$) puddle generated due to charge impurity and disorder created in the CSG lattice as a result of charge transfer from TM to CSG [22].

*cnssks@iacs.res.in

II. EXPERIMENTS

A. Synthesis of the TM-CSG nanocomposite

In the first step, graphene oxide (GO) was synthesized in the usual way as reported earlier [23]. To synthesize CSG 50 ml of aqueous solution of GO was taken in a beaker and ultrasonicated until the temperature rises to 60 °C. Then 5 ml of hydrazine hydrate (N_2H_4 , H_2O) was added dropwise to the solution and further sonicated for 2 h. After 2-h sonication, 10 mg of $NaBH_4$ was added to the solution and kept under ultrasonic vibration for another 4 h. The black product was filtered and washed several times with double distilled water and ethanol and dried in a vacuum oven at 60 °C for 24 h. To synthesize Co and Ni decorated CSG, 25 mg of as synthesized CSG was dispersed in 100 ml of anhydrous DMF (N,N -dimethylformamide) solution and sonicated for 2 h at room temperature. We have synthesized four samples in which two are decorated by cobalt (0.5 and 1 mg) and the other two are decorated by Ni (0.5 and 1 mg) keeping the CSG amount the same. For the Co (1 mg) sample 10 ml of aqueous solution of 1 mg $Co(OAc)_2$ was added slowly under stirring condition for 1.5 h at 80 °C. After cooling to room temperature, the product was washed using a centrifuge at 12 000 rpm and then dispersed in 50 ml of water for hydrothermal treatment at 180 °C for 10 h. The final product was filtered and washed with distilled water and ethanol several times and dried at 60 °C in vacuum overnight. In the last step, the powder sample was reduced in hydrogen atmosphere at 450 °C for 1 h.

The rest of the compositions were synthesized in a similar procedure. For comparison, pristine CSG was also annealed under similar conditions.

B. Characterizations

For characterization of as prepared samples, we have performed x-ray diffraction (XRD) using a Bruker D8 advance diffractometer, Da Vinci model. Raman spectroscopy measurement is carried out by a JYT6400 micro-Raman spectrometer. Atomic force microscopy (AFM) measurement is done in the contact mode by PicoLE AFM equipment (Agilent Corp., USA). X-ray photoelectron spectroscopy (XPS) is investigated by a OMICRON-0571 system under ultrahigh vacuum condition. Microstructural analysis is carried out by JEOL-2011 high-resolution transmission electron microscope. Electrical and magnetotransport measurements are carried out by a physical property measurement system (PPMS). For magnetic measurements, we have used a superconducting quantum interference device magnetometer, Quantum Design MPMS XL-5.

C. Raman analysis for charge-transfer process

To understand the charge transfer from TM (Co, Ni) to CSG, we have investigated Raman spectra of both pristine CSG and TM decorated CSG. It is well known that the G band of CSG downshifts when the CSG surface is surmounted by donor-type atoms, i.e., electron donating groups [24,25]. Figures 1(a) and 1(b) show the Raman spectra of the Co

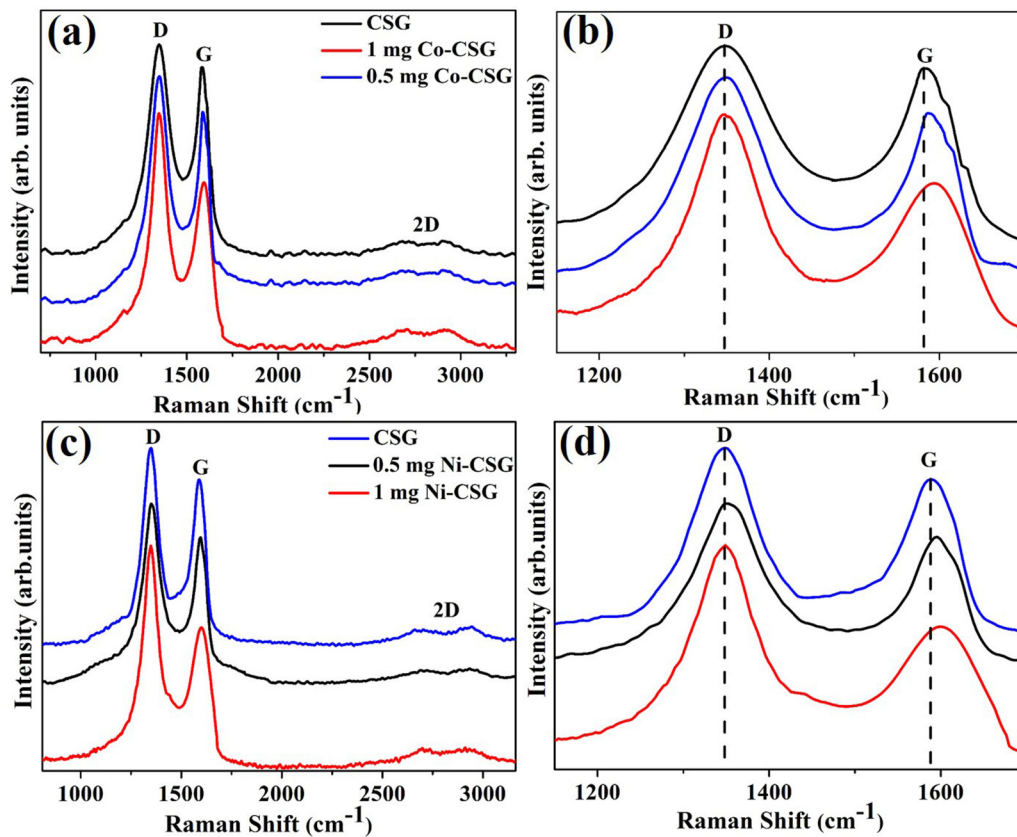


FIG. 1. The Raman spectra (a) pristine CSG and Co-CSG samples, (b) magnified view of (a), (c) pristine CSG and Ni-CSG samples, and (d) magnified view of (c).

decorated sample along with pristine CSG from which it is seen that the G band for pristine CSG appears at 1584.98 cm^{-1} while for 0.5 and 1 mg Co samples these bands are shifted to 1592.70 and 1598.06 cm^{-1} , respectively. However, D bands for the three samples appear in the same position. For Ni decorated samples, the positions of G bands are 1590.35 and 1593.07 cm^{-1} for 0.5 and 1 mg Ni concentrations, respectively, shown in Figs. 1(c) and 1(d). In both cases, the position of the D band in pristine CSG and TM-CSG is 1347.49 cm^{-1} . Therefore, it appears that the position of the G band shifts more and more as we increase the TM concentration, indicating the charge-transfer effect from TM to CSG. The values of $\frac{I_D}{I_G}$ and $\frac{I_{2D}}{I_G}$ of all the samples are given in Table I.

TABLE I. Ratio of peak intensities of D and G bands from Raman analysis.

Composition	$\frac{I_D}{I_G}$	$\frac{I_{2D}}{I_G}$
CSG	1.10	0.16
0.5 mg Co-CSG	1.18	0.15
1 mg Co-CSG	1.41	0.14
0.5 mg Ni-CSG	1.23	0.06
1 mg Ni-CSG	1.61	0.05

D. XPS analysis for verification of charge transfer

For elemental verification of the TM-CSG samples we have carried out full range XPS spectra of 0.5 mg Co-CSG and 1 mg Co-CSG samples as shown in Figs. 2(a) and 2(b),

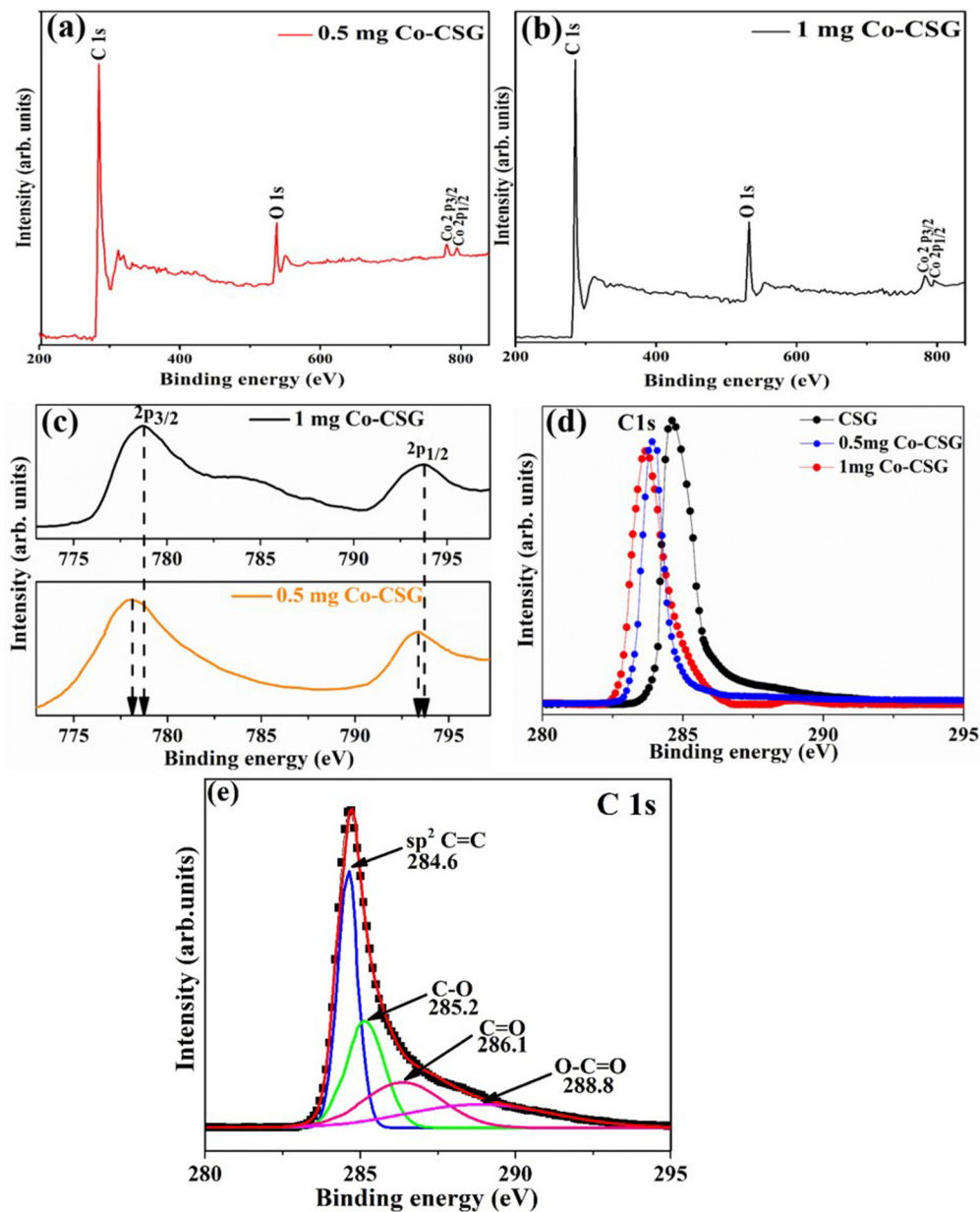


FIG. 2. (a, b) Full range XPS spectra of Co-CSG samples. (c) Comparison of high-resolution XPS spectra for the Co phase. (d) Comparison of high-resolution XPS spectra of C1s for Co-CSG and pristine CSG samples. (e) High-resolution deconvoluted XPS peaks for C1s.

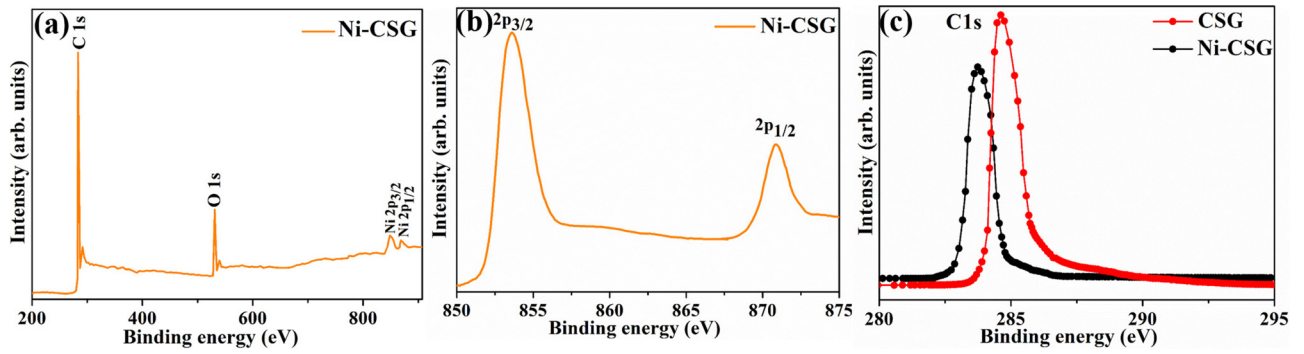


FIG. 3. (a) Full range XPS spectra of the Ni-CSG sample. (b) High-resolution XPS spectrum of the Ni phase. (c) Comparison of high-resolution XPS spectra of $C1s$ for Ni-CSG and pristine CSG.

respectively. From the full range of XPS spectra, the presence of C, O, and Co is verified and no other element has been detected, confirming the purity of the samples. In order to clarify the bonding nature of carbon, we have performed XPS analysis of pristine CSG and deconvoluted the $C1s$ spectrum to verify the presence of different groups, as shown in Fig. 2(e). Among the four peaks, contribution from $C=C$, i.e., sp^2 bonded C, is of the highest intensity, which is positioned at 284.6 eV [26,27]. We have compared the high-resolution Co $2p$ spectra for 0.5 and 1 mg Co-CSG samples as shown in Fig. 2(c). The positions for $2p_{3/2}$ and $2p_{1/2}$ for 1 mg Co-CSG appear at around 778.6 and 793.8 eV, respectively, while for the 0.5 mg Co-CSG sample the peaks are shifted to 778.0 and 793.4 eV, respectively, as shown in Fig. 2(c). The shifts in this case are +0.6 and +0.4 eV for $2p_{3/2}$ and $2p_{1/2}$ states, respectively, with the variation of Co concentration in the two samples. We have also compared the high-resolution $C1s$ spectra for the Co-CSG samples (0.5 and 1 mg) with the pristine CSG as depicted in Fig. 2(d). It is seen that the $C1s$ peak appears at around 283.6 and 283.9 eV for 1 and 0.5 mg Co-CSG samples, which are shifted by -0.9 and -0.6 eV compared to the pristine CSG $C1s$ spectrum that appears at 284.5 eV shown in Fig. 2(c). Next, for the Ni-CSG sample the full range XPS spectrum is shown in Fig. 3(a). The Ni $2p_{3/2}$ and $2p_{1/2}$ high-resolution spectra are given in Fig. 3(b) and show a shift of +0.8 and +0.5 eV, respectively, with the standard value [28,29]. Compared to the pristine CSG $C1s$ spectrum [Fig. 3(c)], the shift for the Ni-CSG $C1s$ peak is -0.8 eV. The reason for the shift in binding energy is due to charge transfer from cobalt to carbon at the interface. As the electrons from the outermost orbital of Co are transferred to the CSG p orbital the binding energy of the electrons of Co increases,

resulting in a shift in binding energy. The opposite process occurs for CSG, where the outermost orbital gains an electron from TM (Co or Ni) via charge transfer and the binding energy of carbon decreases. The shift in binding energies among different concentrations of samples is tabulated in Table II. Thus from XPS analysis the direction of charge transfer can be confirmed from this shift.

E. ICP-OES study for elemental detection

We have carried out inductively coupled plasma optical emission spectrometry (ICP-OES) analysis using a PerkinElmer DV to calculate the percentages of Co and Ni present in the material. First, 2 mg of Co-CSG powder is put into 10 ml of 10% HNO_3 (Suprapur, Merck, 65%) solution, then the Co-CSG solution is ultrasonicated for 40 min in an ultrasonic bath. The concentration of Co-CSG mixed with acid solution is 0.2 mg/ml. Then, 0.1 ml of solution from the above mixer is taken and diluted 100 times using 10 ml of 10% HNO_3 solution. The concentration of Co-CSG becomes 0.002 mg/ml. The solution is diluted further 100 times by the same procedure and the final concentration is 0.0002 mg/ml. We have carried out ICP-OES measurement with the diluted solution containing 0.0002 mg/ml of Co-CSG. We have also prepared another solution of the composite (Ni-CSG) with a concentration of 0.0002 mg/ml by the same procedure [30]. The analysis results are summarized in Table III.

F. Thickness measurement by atomic force microscopy

In order to measure the thickness of CSG layers, we have carried out AFM measurements on TM-CSG samples. For this measurement we have used Si/SiO₂ wafer (Sigma Aldrich) as

TABLE II. Shift in binding energy of the orbitals from XPS analysis.

Sample	Co $2p_{3/2}$ (eV)	Shift (eV)	Co $2p_{1/2}$ (eV)	Shift (eV)	$C1s$ (eV)	Shift (eV)
CSG (pristine)					284.5	
1 mg Co-CSG	778.6	+0.6	793.8	+0.4	283.6	-0.9
0.5 mg Co-CSG	778.0		793.4		283.9	-0.6
Sample	Ni $2p_{3/2}$ (eV)	Shift (eV)	Ni $2p_{1/2}$ (eV)	Shift (eV)	$C1s$ (eV)	Shift (eV)
CSG (pristine)					284.5	-0.8
Ni-CSG	853.6	+0.8	870.9	+0.5	283.7	
Ni standard value	852.8		870.4			

TABLE III. The calculated percentage of elements in the samples obtained from ICP-OES study.

Element	Percentage (%)
Co	5.1
Ni	6.5

substrate. Figures 4(a) and 4(c) show the AFM image of one Co and Ni sample. From selected portions of these images we get the thickness of CSG layers, found to be about 2.6 and 2.3 nm, respectively, as shown in Figs. 4(b) and 4(d). Considering the layer separation of 0.34 nm in CSG, the number of layers in our samples has been estimated as 6, from which we can conclude that as synthesized graphene samples are very thin in nature.

G. XRD analysis for phase detection

Figure 5(a) shows the XRD profile of one Co-CSG sample as that of the Ni-CSG sample. From the XRD profile of both samples we get only a broad peak around $\sim 25.1^\circ$ which corresponds to the (002) plane of CSG and a small hump around 43.6° which arises due to the (100) in-plane lattice of CSG, indicating that both come from CSG [31,32]. As in our TM-CSG samples concentrations Co and Ni are very diluted, there is no such sharp peak of metallic Co or Ni in the composite material. Also, no other oxide peaks of Co and Ni are observed, which verifies the purity of the samples.

H. Transmission electron microscopy for microstructure analysis

Figure 5 shows the overall morphology which is typical of all the samples. Very thin CSG sheets are observed in the TEM micrograph [33,34]. The high-resolution image of pristine CSG shown in Fig. 5(b) clearly features the (002) interlayers with lattice spacing of 0.34 nm, which indicates the characteristic multilayered structure of our chemically synthesized graphene. Figure 5(c) represents the microstructure of 1 mg Co-CSG composition. Figure 5(d) shows its high-resolution image. It is interesting to observe that despite the presence of cobalt in the composite material no evidence of a cobalt nanoparticle is observed in the high-resolution image although in the energy dispersive x-ray analysis (EDAX) trace amounts of TM atoms are observed in the TM-CSG samples as shown in Fig. 6(a). Also, in the case of Ni-CSG composition a similar kind of thin images of CSG layers is observed as shown in Figs. 5(e) and 5(f). In the high-resolution image of Ni-CSG composition no Ni particles are observed. But surprisingly during the EDAX analysis very minute amounts of Co and Ni concentrations are observed with respect to CSG concentration as shown in Figs. 6(a) and 6(b). This is due to the fact that very dilute amounts of cobalt and nickel precursors were taken during synthesis.

III. RESULTS AND DISCUSSION

A. Positive magnetoresistance: Wave-function shrinkage model

To investigate the magnetotransport property of the present series of samples we have measured MR as a function of

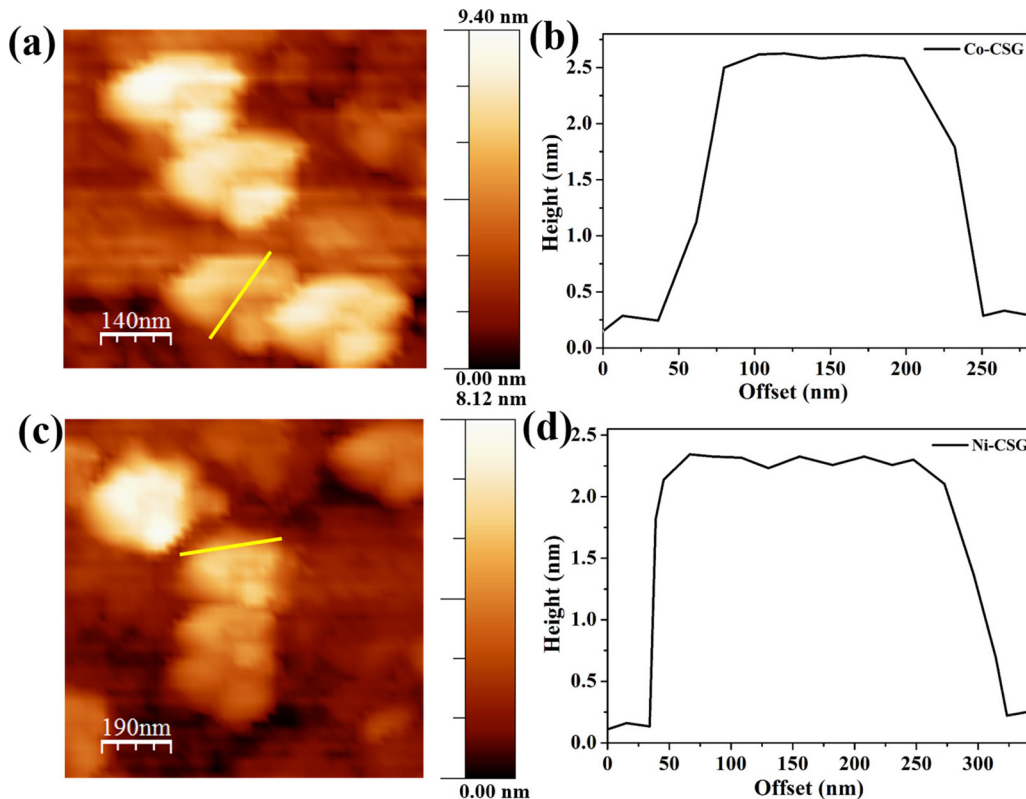


FIG. 4. The AFM image (a) Co-CSG sample, (b) height profile for Co-CSG, (c) Ni-CSG sample, and (d) height profile for Ni-CSG.

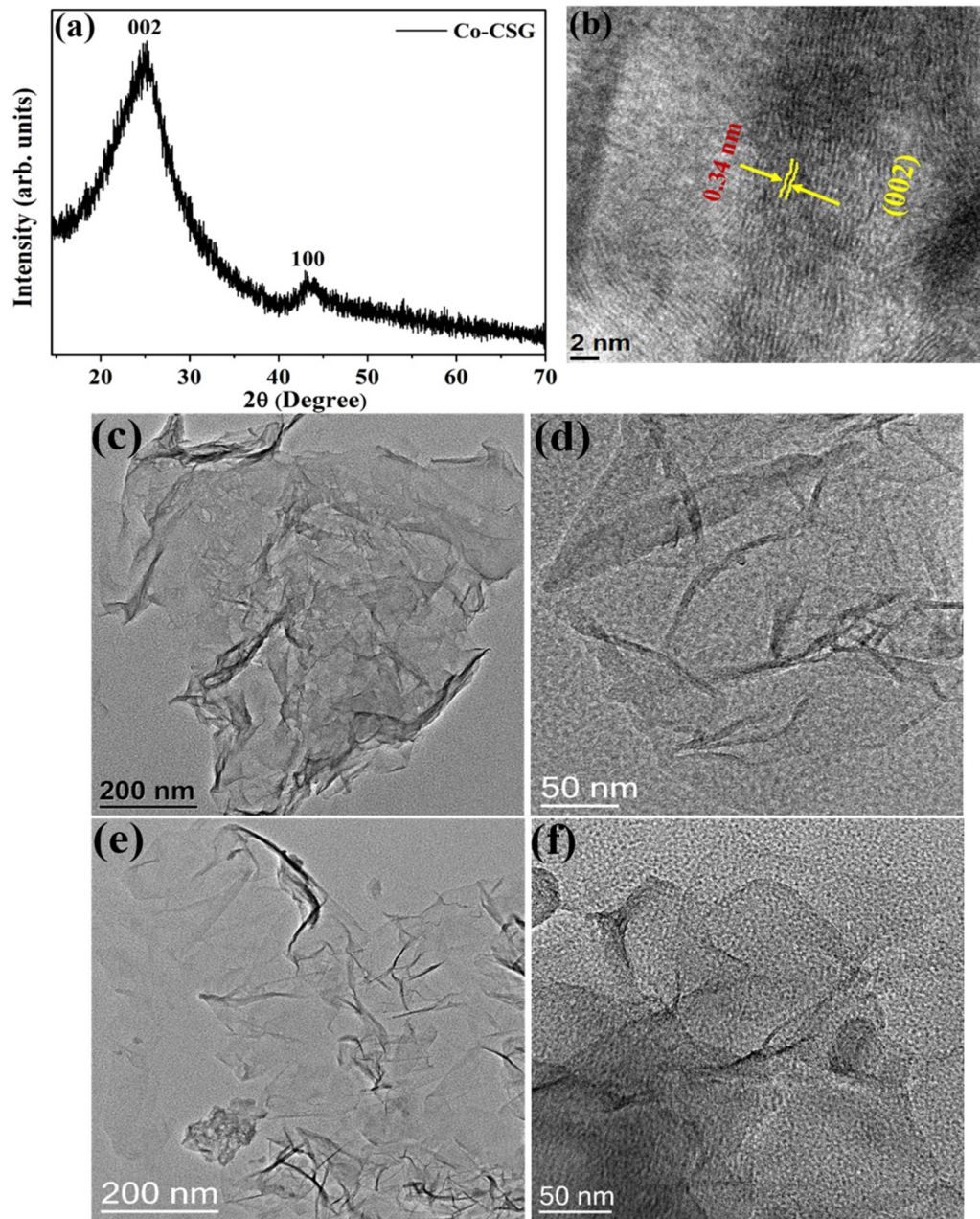


FIG. 5. (a) The XRD profile of a typical Co-CSG sample. (b) The high-resolution TEM micrographs of pristine CSG. (c, d) Co-CSG sample. (e, f) Ni-CSG sample TEM micrograph.

field (up to 9 T) over the temperature range 5–300 K in a standard PPMS system in which cold head (Sumitomo Japan) and a liquid He compressor (Janis, USA) for the 300–5 K temperature range were used with a superconducting magnet with maximum field up to ± 9 T. A Lakeshore model 335 was the temperature controller. For current source meter a Keithley 2601 was used and for voltage drop measurement a Keithley 2182A nanovoltmeter was used. Data acquisition was done by a LABVIEW 11 software interface. For magnetoresistance and resistivity measurement we used a circular pellet made of powder samples with diameter 6 mm and thickness 0.8 mm. This was prepared in a hydraulic press under a pressure of 3 ton. Standard four probe technique was used during measurement. For electrode purposes gold wires (30 μm) were

attached using conductive graphite paste (Alfa Aesar). The separation between the Au electrode wires was 0.44 mm. The measurement arrangement is schematically shown in Fig. 7. The sample was placed vertically inside the PPMS sample holder such that the magnetic field remains perpendicular to the surface of the sample. Thus we used the current-in-plane method for contact geometry.

The as synthesized bulk CSG shows a high positive magnetoresistance ($\sim 39\%$) presented in Fig. 8 which decreases with increasing temperature usually. This huge positive magnetoresistance is explained on the basis of a modified wave-function shrinkage model, where the contraction of the electronic wave function at impurity centers in the magnetic field causes a reduction in the hopping probability between two sites and

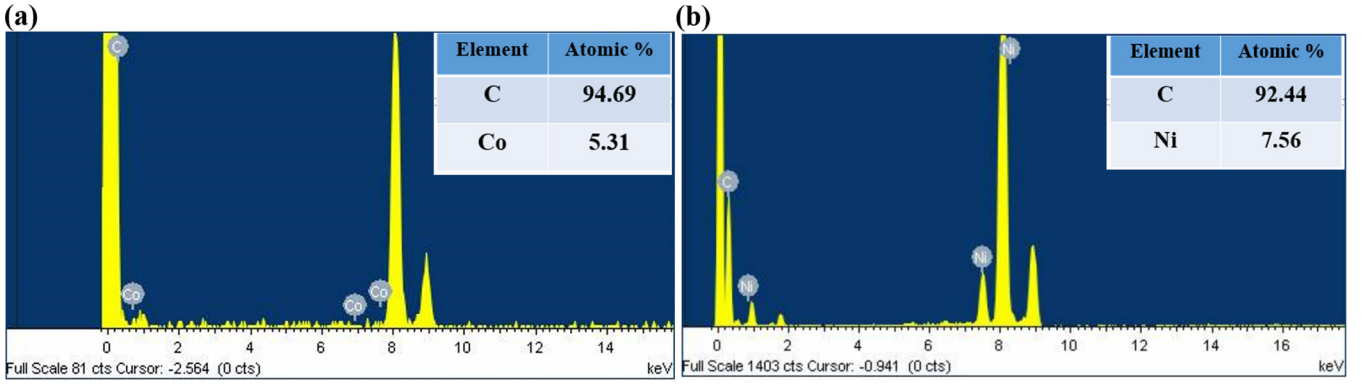


FIG. 6. The EDAX pattern of the (a) Co-CSG and (b) Ni-CSG sample.

results in a positive MR [35]. In this case the dilute concentration of TM (Co, Ni) placed on the graphene matrix distorts the band structure and acts as an impurity center.

In the wave-function shrinkage model, the ratio of $R(H,T)/R(0,T)$ can be described by Eq. (1):

$$\frac{R(H, T)}{R(H, 0)} = \exp\{\xi_C(0)[\xi_C(H)/\xi_C(0) - 1]\} \quad (1)$$

where $\xi_C = (T_0/T)^{1/3}$ for the two-dimensional (2D) Mott variable range hopping (VRH) electrical conduction mechanism, $\xi_C(H)/\xi_C(0)$, is the normalized hopping probability parameter and is a function of H/H_C for the Mott VRH electrical conduction mechanism. H_C is the fitting parameter given by Eq. (2) for the Mott VRH electrical conduction mechanism:

$$H_C = 6\hbar/ea_0^2(T_0/T)^{1/3}. \quad (2)$$

In the low-field limit Eq. (1) simplifies to

$$\frac{R(H, T)}{R(H, 0)} \approx 1 + t_2 \frac{H^2}{H_C^2} \left(\frac{T_0}{T}\right)^{1/3}$$

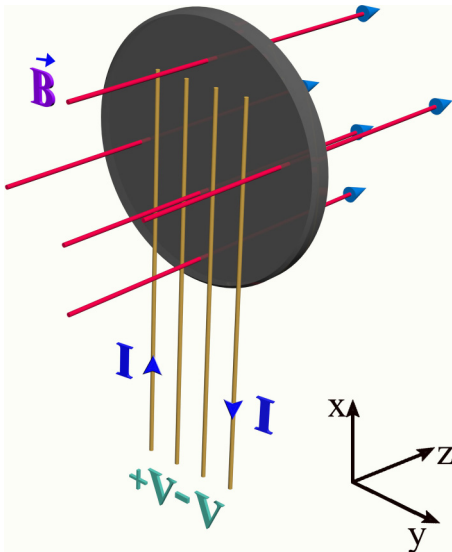


FIG. 7. Schematic diagram of contact geometry for transport measurements.

and the MR is defined by Eq. (3):

$$\text{MR} \approx t_2 \frac{H^2}{H_C^2} \left(\frac{T_0}{T}\right)^{1/3} = t_2 \frac{e^2 a_0^4}{36\hbar^2} \left(\frac{T_0}{T}\right) H^2 \quad (3)$$

with T_0 being the Mott characteristic temperature given by $T_0 = \frac{24}{[\pi k_B N(E_F) a_0^2]}$. Here, $t_2 = (5/2016) \times 36 \sim 0.89$ is a numerical constant, e is the electronic charge, \hbar is Planck's constant, a_0 is the localization length, and k_B and $N(E_F)$ are the Boltzmann constant and density of states at the Fermi level. It is to be mentioned that the wave-function shrinkage model contains two parameters a_0 and $N(E_F)$ which are field dependent, although in previous reports these parameters were considered as field independent during study of MR as a function of field. Therefore, to investigate the magnetoresistance behavior as a function of field we have incorporated an additional parameter k with a negative sign to the power of H to introduce field dependence in a_0 and $N(E_F)$:

$$\text{MR} = \left(\frac{1.9 \times 10^{29} a_0^2}{N(E_F)}\right) \left(\frac{H^{2-k}}{T}\right). \quad (4)$$

Justification behind this negative sign of parameter k lies in the fact that the expression for MR shown in Eq. (4) contains the ratio $a_0^2/N(E_F)$ which decreases with increasing field. The solid lines are the theoretical curves as obtained by Eq. (4) whereas different symbols represent the experimental plot at different temperatures. From Fig. 8 it is seen that the positive MR data of CSG are well fitted by the wave-function shrinkage model. According to Eq. (3), the localization length a_0 could be obtained using the MR value as given by Eq. (5):

$$a_0^4 = \frac{36\hbar^2 \text{MR}}{t_2 e^2} \left(\frac{T_0}{T}\right)^{-1} H^{-2}. \quad (5)$$

Given the value of a_0 , the density of states at the Fermi level $N(E_F)$ can be calculated using Eq. (6) as

$$N(E_F) = \frac{24}{\pi k_B T_0 a_0^2}. \quad (6)$$

The average hopping length R_{hop} can be calculated using Eq. (7) with the value of T_0 and of a_0 as [36]

$$R_{\text{hop}} = 3/8 (T_0/T)^{1/3} a_0. \quad (7)$$

The values of the parameters extracted from the fitting procedure are summarized in Table IV. From the table it is

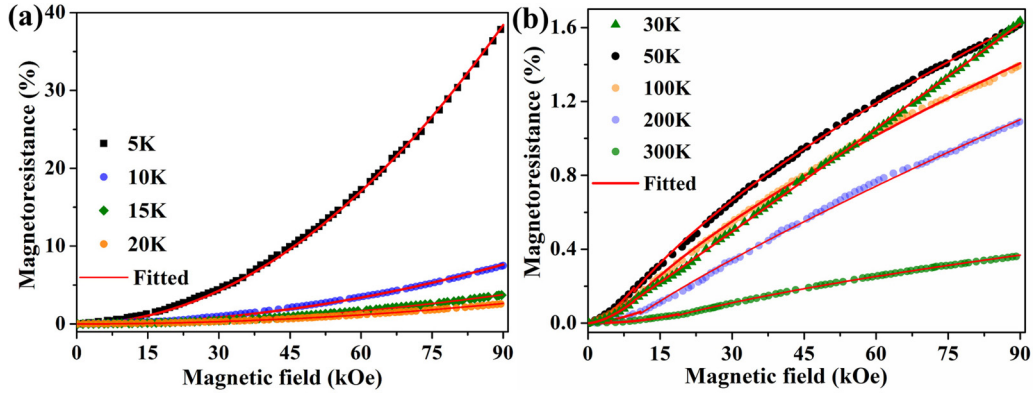


FIG. 8. Magnetoresistance of pristine CSG samples (a) at low temperature and (b) at high temperature.

seen that for all samples the ratio of parameters $a_0^2/N(E_F)$ decreases with temperature, however the parameter k increases with temperature. Therefore, from the variation of parameters a_0 , N_{E_f} , and k with temperature it is observed that the wave-function shrinkage model breaks down as temperature goes up to room temperature. It is also to be noted that the values of these parameters are estimated at different fields keeping temperature constant as shown in Table IV. The value of a_0 (localization length) decreases, however N_{E_f} (density of states at Fermi level) increases with increasing field and is found to be consistent with the literature results investigated in other systems [37]. The effect of wave-function shrinkage

under application of higher magnetic field results in decrease in hopping distance R_{hop} as shown in Table V.

B. Negative magnetoresistance: Formation of an e - h puddle due to charge localization

So far we have discussed the positive MR behavior of virgin CSG on the basis of the wave-function shrinkage model. In this section we will discuss the interesting results of MR behavior in TM-CSG samples. Figures 9(a) and 9(b) show the MR behavior of the Co-CSG (0.5 mg of Co) in the low-temperature (5–30 K) and high-temperature (50–300 K)

TABLE IV. Parameters obtained after fitting the MR data with Eq. (4).

Pristine CSG									
T	$\frac{a_0^2}{N(E_F)}$ (J cm^4)		k		T	$\frac{a_0^2}{N(E_F)}$ (J cm^4)		k	
5 K	4.02×10^{-35}	$\pm 2.11 \times 10^{-37}$	0.04	± 0.002	50 K	4.89×10^{-36}	$\pm 5.27 \times 10^{-38}$	1.50	± 0.12
10 K	2.72×10^{-35}	$\pm 5.42 \times 10^{-37}$	0.052	± 0.008	100 K	1.97×10^{-36}	$\pm 1.29 \times 10^{-38}$	1.52	± 0.18
15 K	1.85×10^{-35}	$\pm 1.81 \times 10^{-37}$	0.068	± 0.001	200 K	7.12×10^{-37}	$\pm 2.07 \times 10^{-38}$	1.56	± 0.07
20 K	8.58×10^{-36}	$\pm 9.51 \times 10^{-37}$	0.07	± 0.005	300 K	4.63×10^{-37}	$\pm 1.54 \times 10^{-38}$	1.57	± 0.11
30 K	7.5×10^{-36}	$\pm 6.52 \times 10^{-37}$	1.47	± 0.08					
0.5 mg Ni-CSG			1 mg Ni-CSG		1 mg Co-CSG		0.5 mg Co-CSG		
T	$\frac{a_0^2}{N(E_F)}$ (J cm^4)	k	$\frac{a_0^2}{N(E_F)}$ (J cm^4)	k	$\frac{a_0^2}{N(E_F)}$ (J cm^4)	k	$\frac{a_0^2}{N(E_F)}$ (J cm^4)	k	
5 K	1.18×10^{-34}	0.06	6.57×10^{-35}	0.095	2.42×10^{-38}	0.017	1.04×10^{-35}	0.01	
	$\pm 1.04 \times 10^{-37}$	± 0.004	$\pm 1.11 \times 10^{-36}$	± 0.010	$\pm 1.12 \times 10^{-40}$	± 0.002	$\pm 7.08 \times 10^{-38}$	± 0.001	
10 K	3.77×10^{-35}	0.08	3.76×10^{-35}	0.03	8.31×10^{-39}	0.032	8.85×10^{-36}	0.06	
	$\pm 1.71 \times 10^{-37}$	± 0.005	$\pm 2.2 \times 10^{-37}$	± 0.007	$\pm 2.49 \times 10^{-41}$	± 0.009	$\pm 4.79 \times 10^{-38}$	± 0.008	
15 K	8.21×10^{-36}	0.13	1.71×10^{-35}	0.05	5.69×10^{-39}	0.04	4.89×10^{-36}	0.087	
	$\pm 6.56 \times 10^{-38}$	± 0.002	$\pm 1.44 \times 10^{-36}$	± 0.008	$\pm 5.07 \times 10^{-41}$	± 0.007	$\pm 1.10 \times 10^{-39}$	± 0.010	
20 K	5.26×10^{-36}	0.14	1.27×10^{-35}	0.094	2.94×10^{-39}	0.042	2.41×10^{-36}	0.08	
	$\pm 2.25 \times 10^{-38}$	± 0.005	$\pm 6.88 \times 10^{-37}$	± 0.005	$\pm 7.51 \times 10^{-41}$	± 0.005	$\pm 1.05 \times 10^{-39}$	± 0.001	
30 K	1.87×10^{-36}	0.143	3.21×10^{-36}	0.102			4.60×10^{-37}	0.085	
	$\pm 2.65 \times 10^{-38}$	± 0.001	$\pm 1.61 \times 10^{-38}$	± 0.009			$\pm 1.51 \times 10^{-39}$	± 0.008	

TABLE V. Calculated parameters a_0 , $N(E_F)$, and R_{hop} .

CSG (5 K)	0.15T	1T	2T	4T	6T	9T
a_0 (nm)	67.71	52.24	45.31	41.43	40.87	40.71
$N(E_F)(\text{J}^{-1} \text{cm}^{-2})$	8.29×10^{29}	1.37×10^{30}	1.82×10^{30}	2.22×10^{30}	2.24×10^{30}	2.26×10^{30}
R_{hop} (nm)	364.41	281.92	244.63	223.61	220.86	219.78
1 mg Ni-CSG (5 K)	2T	4T	6T	9T		
a_0 (nm)	53.21	51.53	50.11	49.72		
$N(E_F)(\text{J}^{-1} \text{cm}^{-2})$	1.23×10^{31}	1.31×10^{31}	1.38×10^{31}	1.41×10^{31}		
R_{hop} (nm)	136.29	131.84	128.26	127.23		
1 mg Co-CSG (5 K)	2T	4T	6T	9T		
a_0 (nm)	43.23	42.21	41.92	41.71		
$N(E_F)(\text{J}^{-1} \text{cm}^{-2})$	3.24×10^{31}	3.40×10^{31}	3.45×10^{31}	3.48×10^{31}		
R_{hop} (nm)	92.02	89.89	89.24	88.81		

regions, respectively. In the low-temperature region, the behavior is similar to CSG and the positive MR has been explained on the basis of the wave-function shrinkage model, however in the high-temperature region the behavior is very different and a negative MR which increases with temperature is observed. It is also to be pointed out that a giant enhancement (from 0.9 to 33%) in negative MR is noticed with increasing Co concentration only from 0.5 to 1 mg. Similar results are obtained in the case of Ni-CSG (from 0.6 to 28%) as shown in Fig. 10. The nature of this huge change in negative MR in the present TM-CSG samples is different from that obtained in the case of spin orbit coupling or spin-spin scattering, in which cases the variation of MR in the low-field

region is much faster than that in the high-field region. In our case the negative MR value increases slowly in the low-field region, however in the high-field region it increases much faster. In addition, unusually, the negative MR increases with increasing temperature.

Therefore, we explain our negative MR results by considering an e - h puddle generated on the CSG surface due to charge impurity as a result of charge-transfer effect [38,39] from TM to CSG and disorder created by TM (Co, Ni) at the CSG lattice which considerably affects the electronic and transport properties of graphene around the Dirac point. The presence of Ni and Co on the CSG surface breaks the homogeneity of the electron cloud on the CSG surface due to additional disorder

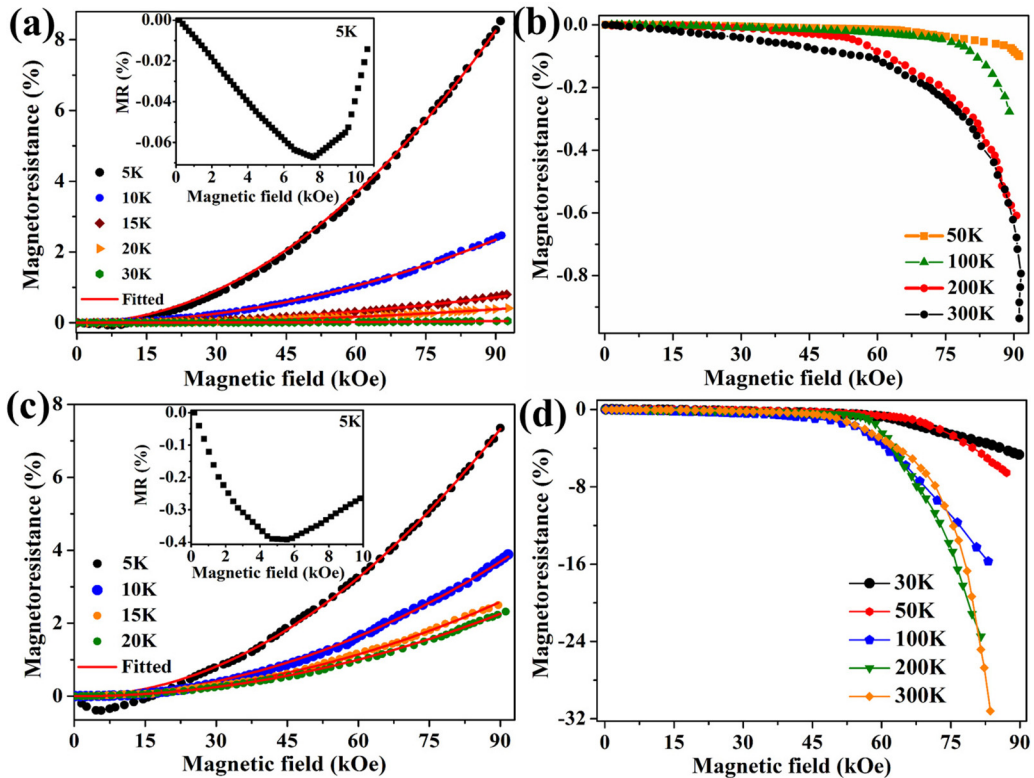


FIG. 9. (a, b) Magnetoresistance of 0.5 mg Co-CSG at low and high temperatures, respectively. (c, d) Magnetoresistance of 1 mg Co-CSG at low and high temperatures, respectively. Inset: The negative MR at 5 K for both the samples.

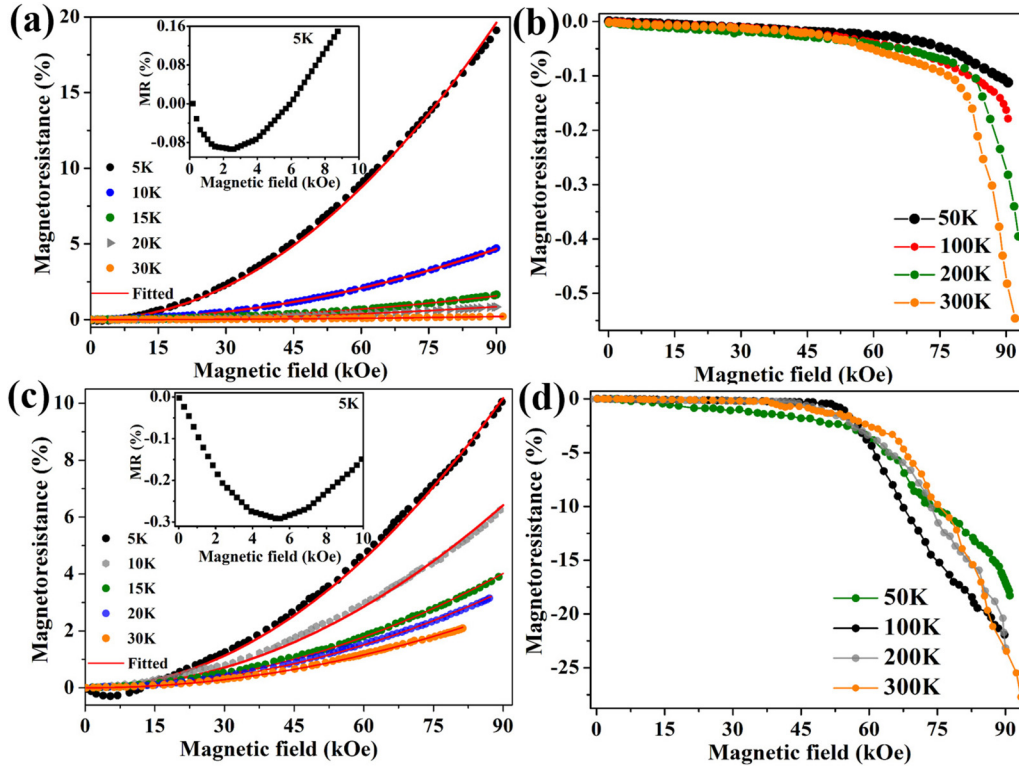


FIG. 10. (a, b) Magnetoresistance of 0.5 mg Ni-CSG at low and high temperatures, respectively. (c, d) Magnetoresistance of 1 mg Ni-CSG at low and high temperatures, respectively. Inset: The negative MR at 5 K for both the samples.

and charge impurity coming from TM to CSG. Because of the formation of these e - h puddles the electrical resistance of the sample increases. Under application of magnetic field these puddles in the graphene surface tend to merge together. At high enough magnetic field B , electron-hole puddles are destroyed with the formation of a more homogeneous electron cloud, resulting in negative MR as observed in our sample. From Figs. 9(b), 9(d), 10(b), and 10(d) it is seen that the negative MR increases with increasing temperature, which confirms that the observed negative MR in the present TM-CSG samples is not due to spin-orbit coupling or spin-spin scattering.

Therefore, to explain the negative MR and anomalous enhancement of MR with increasing temperature in the present samples we have considered the charge-transfer effect at the interface of TM and CSG creating a potential barrier and an antiferromagnetic interaction when a TM atom is placed on the CSG surface. This charge-transfer effect along with the potential barrier and the magnetic interaction at the TM-CSG

interface has been investigated extensively both theoretically as well as experimentally during the last few years [5,40]. We have considered that the charge impurity transferred from TM together with the disorder created in the CSG lattice due to the presence of TM produce local distortion (inhomogeneity) of the electron cloud with the formation of an e - h puddle in the CSG lattice. The size of the puddle is given by [41]

$$d_p = \frac{r_{TG}(n_2) - r_{TG}(n_1)}{2n_c} - 2r_{BG} \quad (8)$$

with $r_{TG} = \frac{\sqrt{n_{TG}}}{B}$. Here, r_{TG} and r_{BG} represent the cyclotron radii near and away from the TM, respectively; n_1 and n_2 represent the charge densities in two regions; and n_c gives the number of orbits. If r_{TG} and r_{BG} are smaller than the puddle size then all the electrons will be scattered and increase the resistance value. Putting r_{TG} as a function of magnetic field in Eq. (8) we get the expression for puddle size as

$$d_p = \frac{\sqrt{n_2(TG)} - \sqrt{n_1(TG)}}{2n_c B} - 2r_{BG}. \quad (9)$$

TABLE VI. Comparison of coercivity values of different composition at different temperatures.

Sample	Temperature (K)	Forward coercivity (Oe)	Reverse coercivity (Oe)	Average coercivity (Oe)
1 mg Co-CSG	2	120	135	128
	5	42	45	44
0.5 mg Co-CSG	2	31	41	36
	5	20	60	40
1 mg Ni-CSG	2	171	191	181
	5	64	57	61

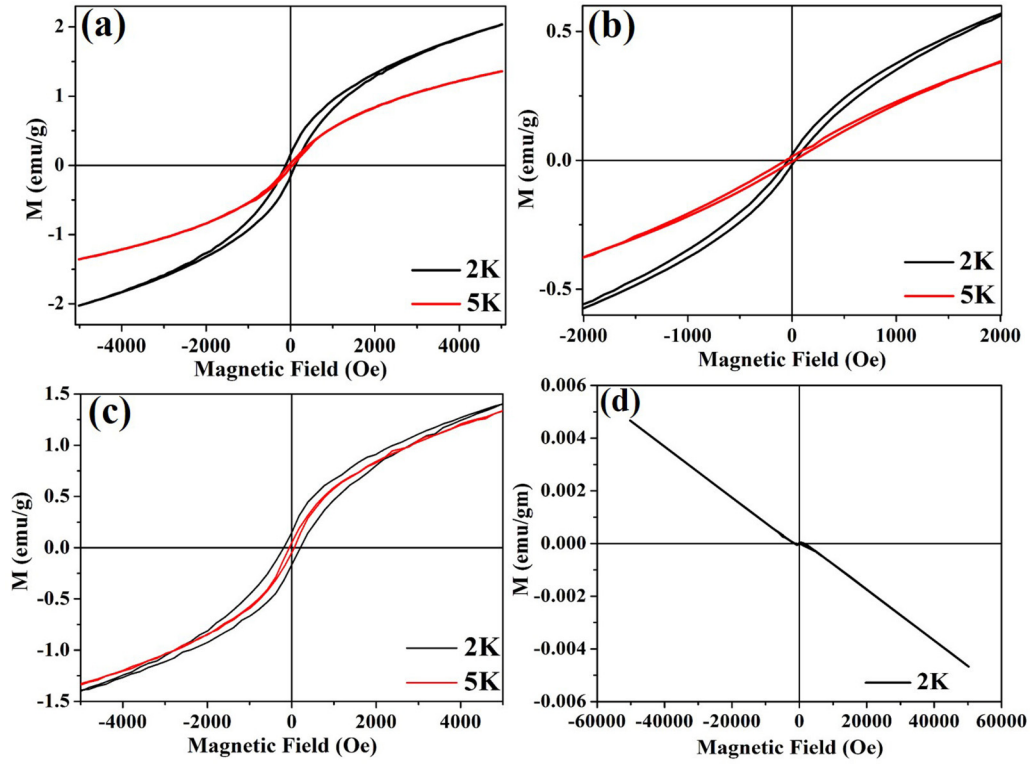


FIG. 11. The M-H hysteresis loops for (a) 1 mg Co-CSG, (b) 0.5 mg Co-CSG, (c) 1 mg Ni-CSG, and (d) pristine CSG.

Therefore, it appears that both r_{TG} and d_P decrease with increasing magnetic field. To explain the negative MR we have considered an expression for d_P , from which it is seen that the size of the e - h puddle decreases with increasing magnetic field, giving rise to a lower resistance value as a result of lower scattering probability and vice versa. Temperature-dependent anomalous MR is also explained using expressions for r_{TG} and d_P . From the expression, it is seen that r_{TG} increases with increasing temperature due to increasing carrier density. As r_{TG} increases, probability of scattering with the puddle decreases, resulting in lowering of the resistance value [41].

C. Hysteresis curves

Another interesting point to be noted is that in the low-temperature region where MR behavior follows the

wave-function shrinkage model a small negative MR is noticed in the low-field limit as shown in Figs. 9(a), 9(c), 10(a), and 10(c). To explain this small negative MR of TM (Co and Ni) decorated CSG we have carried out magnetization as a function of field. Ferromagnetic hysteresis loops shown in Fig. 11 are observed at temperatures 2 and 5 K. The coercivities of all three samples are shown in Table VI. This weak ferromagnetic ordering arises due to interaction among the magnetic moments of the charge impurities transferred from TM to CSG. With increasing concentration of TM, better loops with higher coercivity are noticed. It is also interesting that though the concentration of TM is very dilute the saturation magnetic moments of the TM-CSG samples are quite high (~ 2 emu/g for 1 mg Co-CSG, 1.5 emu/g for Ni-CSG, and 0.6 emu/g for 0.5 mg Co-CSG). The reason for such high moments in spite of using very dilute transition

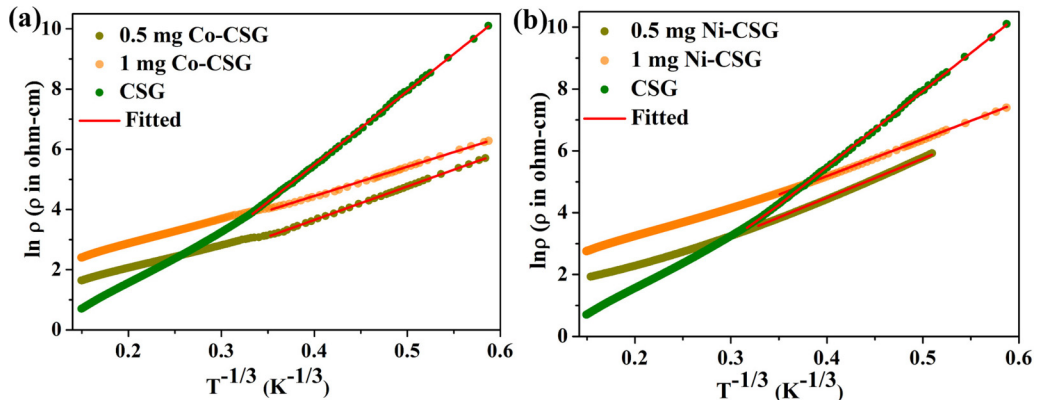


FIG. 12. The $\ln \rho$ vs $T^{-1/3}$ curve for (a) pristine CSG and Co-CSG and (b) pristine CSG and Ni-CSG.

TABLE VII. Parameters obtained after fitting with the $\ln \rho$ vs $T^{-1/3}$ graph by Eq. (10).

Mott characteristic temperature	Pristine CSG	0.5 mg Co-CSG	1 mg Co-CSG	0.5 mg Ni-CSG	1 mg Ni-CSG
T_0 (K)	14796.31	1378.73	915.52	2048.31	1594.33

metal is the charge-transfer effect at the interface of graphene and transition metal. The generation of high ferromagnetic ordering due to charge-transfer effect is also observed earlier [10]. The magnetic spins related to charge impurity act as spin scattering centers in the CSG lattice and a negative MR is observed in the very-low-temperature region. Therefore, in the TM-CSG samples, in the low-temperature limit, there is a competition between wave-function shrinkage possessing positive MR and spin-spin scattering giving rise to negative MR. With increasing field wave-function shrinkage is dominated over spin-spin scattering and the overall MR becomes positive after a certain field. It is also to be noted that this negative MR in the low-temperature region and at low field has not been observed in pristine CSG but only in TM-CSG and increases with increasing TM concentration.

D. Temperature-dependent resistivity: The electrical conduction mechanism

So far we have discussed the detailed MR behavior of TM-CSG along with pristine CSG. The MR behavior in CSG follows the wave-function shrinkage model, however in the case of TM-CSG magnetoresistance arises due to wave-function shrinkage in the low-temperature region and the huge negative MR arises due to the e - h puddle generated in CSG as a result of charge impurity and disorder. Another supportive result to ensure the existence of the e - h puddle and the wave-function shrinkage to be operative in the present systems is the VRH, which usually governs the overall charge transport.

Figure 12 shows the resistivity as a function of temperature (R - T) of the TM-CSG along with pristine CSG. From the figure it is noticed that the resistivity of CSG is higher compared to TM-CSG in the low-temperature region but in the high-temperature region it is lower. It is also to be noted that resistivity is increasing with increasing function of TM concentration. We have investigated the R - T data of our sample by several models such as activating, VRH, etc., and we have seen that the data are best fitted with the VRH model in the 2D system given by [42]:

$$\rho = \rho_0 \exp\left(\frac{T_0}{T}\right)^{1/3} \quad (10)$$

where T_0 is the Mott characteristic temperature. It is seen that the data are well fitted up to temperature ~ 30 K (precisely, 31 K for CSG and 25 and 22 K for TM-CSG samples with 0.5 mg Co and 1 mg Co concentration). The solid lines represent the theoretical lines obtained by using Eq. (10) and the solid symbols are the experimental data. The values of the parameters extracted from the fitted procedure are summarized in Table VII. It is therefore seen that the charge transport followed by VRH in the low-temperature region is consistent with the MR behavior which is governed by the wave-function shrinkage model. As we mentioned in the previous section, with increasing temperature the e - h puddle is generated due to charge impurity and disorder created as a result of the presence of the TM atom, and the resistivity of TM-CSG increases much faster compared to CSG as shown in Fig. 12. It is also to be noted that with increasing Co concentration resistivity further increases because of higher disorder and charge impurity created in the CSG lattice. The same behavior is observed in Ni-CSG samples.

IV. CONCLUSION

In conclusion, using very dilute TM decorated CSG, large magnetoresistance along with good magnetic ordering over the temperature range 5–300 K and magnetic field up to 9 T is observed in this case. In the low-temperature region the charge transport is explained by VRH, which is also in accordance with the wave-function shrinkage model. The transition from large positive to negative magnetoresistance has been explained using the wave-function shrinkage model and electron-hole puddle generated in CSG as a result of charge transfer from TM to CSG. The magnetic hysteresis loop observed in the low-temperature region also confirms the charge-transfer effect in CSG that gives a high amount of magnetic moment to such a dilute system.

ACKNOWLEDGMENTS

C.M. and S.B. acknowledge the Department of Science and Technology (DST) INSPIRE, New Delhi, for awarding their fellowships. S.K.S. acknowledges DST, New Delhi, Government of India for the infrastructural facility. We are thankful to Prof. Masahiro Yamashita, Prof. Keiichi Katoh, Dr. Goulven Cosquer, and Mr. Mohammad Rasel Mian of the Department of Chemistry, Graduate School of Science, Tohoku University for the magnetic measurement facilities.

- [1] A. K. Geim and I. V. Grigorieva, *Nature (London)* **499**, 419 (2013).
- [2] K. S. Novoselov, V. Fal, and L. Colombo, *Nature (London)* **490**, 192 (2012).
- [3] M. Baskey and S. K. Saha, *Adv. Mater.* **24**, 1589 (2012).
- [4] N. Atodiresei, J. Brede, P. Lazic, V. Caciuc, G. Hoffmann, R. Wiesendanger, and S. Blugel, *Phys. Rev. Lett.* **105**, 066601 (2010).

- [5] X. Liu, C. Z. Wang, Y. X. Yao, W. C. Lu, M. Hupalo, M. C. Tringides, and K. M. Ho, *Phys. Rev. B* **83**, 235411 (2011).
- [6] Y. S. Dedkov and M. Fonin, *New J. Phys.* **12**, 125004 (2010).
- [7] A. M. Shikin, A. G. Rybkin, D. Marchenko, A. A. Rybkina, M. R. Scholz, O. Rader, and A. Varykhalov, *New J. Phys.* **15**, 013016 (2013).
- [8] Y. S. Dedkov, M. Fonin, U. Rudiger and C. Laubschat, *Phys. Rev. Lett.* **100**, 107602 (2008).

- [9] M. Weser, Y. Rehder, K. Horn, M. Sicot, M. Fonin, A. B. Preobrajenski, E. N. Voloshina, E. Goering and Yu. S. Dedkov, *Appl. Phys. Lett.* **96**, 012504 (2010).
- [10] S. Mandal and S. K. Saha, *Appl. Phys. Lett.* **105**, 022402 (2014).
- [11] S. Bhattacharya, D. Dinda, B. K. Shaw, S. Dutta, and S. K. Saha, *Phys. Rev. B* **93**, 184403 (2016).
- [12] A. Debnath, S. Bhattacharya, and S. K. Saha, *Phys. Rev. B* **96**, 214433 (2017).
- [13] V. A. Rigo, T. B. Martins, A. J. R. da Silva, A. Fazzio, and R. H. Miwa, *Phys. Rev. B* **79**, 075435 (2009).
- [14] O. Rader, A. Varykhalov, J. Sanchez-Barriga, D. Marchenko, A. Rybkin, and A. M. Shikin, *Phys. Rev. Lett.* **102**, 057602 (2009).
- [15] B. Uchoa, C.-Y. Lin, and A. H. Castro Neto, *Phys. Rev. B* **77**, 035420 (2008).
- [16] H. Sevincli, M. Topsakal, E. Durgun, and S. Ciraci, *Phys. Rev. B* **77**, 195434 (2008).
- [17] Y. Mao, J. Yuan, and J. Zhong, *J. Phys.: Condens. Matter* **20**, 115209 (2008).
- [18] A. Varykhalov and O. Rader, *Phys. Rev. B* **80**, 035437 (2009).
- [19] S. Bhattacharya, E. M. Kumar, R. Thapa, and S. K. Saha, *Appl. Phys. Lett.* **110**, 032404 (2017).
- [20] S. Mandal and S. K. Saha, *Nanoscale* **4**, 986 (2012).
- [21] A. J. Akhtar, A. Gupta, D. Chakravorty, and S. K. Saha, *AIP Advances* **3**, 072124 (2013).
- [22] J. M. Poumirol, W. Escoffier, A. Kumar, M. Goiran, B. Raquet and J. M. Broto, *New J. Phys.* **12**, 083006 (2010).
- [23] W. S. Hummers and R. E. Offeman, *J. Am. Chem. Soc.* **80**, 1339 (1958).
- [24] B. Das, R. Voggu, C. S. Rout, and C. N. R. Rao, *Chem. Commun.* **0**(41), 5155 (2008).
- [25] C. N. R. Rao, K. Biswas, K. S. Subrahmanyam, and A. Govindaraj, *J. Mater. Chem.* **19**, 2457 (2009).
- [26] A. Ganguly, S. Sharma, P. Papakonstantinou, and J. Hamilton, *J. Phys. Chem. C* **115**, 17009 (2011).
- [27] J. Zhang, H. Yang, G. Shen, P. Cheng, J. Zhang, and S. Guo, *Chem. Commun.* **46**, 1112 (2010).
- [28] C. Zhou, J. A. Szpunar, and X. Cui, *ACS Appl. Mater. Interfaces* **8**, 15232 (2016).
- [29] L. Fan, P. F. Liu, X. Yan, L. Gu, Z. Z. Yang, H. G. Yang, S. Qiu, and X. Yao, *Nat. Commun.* **7**, 10667 (2016).
- [30] S. Bag, S. Bhattacharya, D. Dinda, M. V. Jyothirmai, R. Thapa, and S. K. Saha, *Phys. Rev. B* **98**, 014109 (2018).
- [31] G. Wang, J. Yang, J. Park, X. Gou, B. Wang, H. Liu, and J. Yao, *J. Phys. Chem. C* **112**, 8192 (2008).
- [32] H. Saleem, M. Haneef, and H. Y. Abbas, *Mater. Chem. Phys.* **204**, 1 (2018).
- [33] Y. Liu, Q. Feng, Q. Xu, M. Li, N. Tang, and Y. Du, *Carbon* **61**, 436 (2013).
- [34] B. Gupta, N. Kumar, K. Panda, S. Dash, and A. K. Tyagi, *Sci. Rep.* **6**, 18372 (2016).
- [35] T.-I. Su, C.-R. Wang, S.-T. Lin, and R. Rosenbaum, *Phys. Rev. B* **66**, 054438 (2002).
- [36] Y. Long and Z. Chen, *Appl. Phys. Lett.* **85**, 1796 (2004).
- [37] H. Gu, J. Guo, R. Sadu, Y. Huang, N. Haldolaarachchige, D. Chen, D. P. Young, S. Wei, and Z. Guo, *Appl. Phys. Lett.* **102**, 212403 (2013).
- [38] K. L. Chiu, M. R. Connolly, A. Cresti, J. P. Griffiths, G. A. C. Jones, and C. G. Smith, *Phys. Rev. B* **92**, 155408 (2015).
- [39] G. Schubert and H. Fehske, *Phys. Rev. Lett.* **108**, 066402 (2012).
- [40] X. Liu, C. Z. Wang, M. Hupalo, W. C. Lu, M. C. Tringides, Y. X. Yao, and K. M. Hoa, *Phys. Chem. Chem. Phys.* **14**, 9157 (2012).
- [41] S. P. Milovanović and F. M. Peeters, *Nanotechnology* **27**, 105203 (2016).
- [42] N. F. Mott, *Conduction in Non-Crystalline Materials* (Clarendon Press, Oxford, 1993).